Carbon 98 (2016) 557–566

Contents lists available at ScienceDirect

Carbon

journal homepage: www.elsevier.com/locate/carbon

Silver particles modified carbon nanotube paper/glassfiber reinforced polymer composite material for high temperature infrared stealth camouflage

Hetao Chu [a], Zhichun Zhang [a], Yanju Liu [b], Jinsong Leng [a, *]

[a] Center for Composite Materials and Structures, No. 2 YiKuang Street, Science Park of Harbin Institute of Technology (HIT), Harbin, 150080, PR China
[b] Department of Aerospace Science and Mechanics, No. 92 West DaZhi Street, Harbin Institute of Technology (HIT), Harbin, 150001, PR China

ARTICLE INFO

Article history:
Received 29 September 2015
Received in revised form
9 November 2015
Accepted 11 November 2015
Available online 23 November 2015

ABSTRACT

The high temperature infrared stealth glassfiber reinforced polymer composite based on silver particles modified carbon nanotube paper (SMCNP) material is fabricated successfully by a facile method, which possesses thin, lightweight, broad wavelength band and low infrared emissivity features. The conductivity increases 673% after being modified by small amount silver particles retaining the original mechanical property. Infrared emissivity decreases more than 38.9–55.7% from 0.85 to 0.65 in 3–5 μm and 0.45 to 0.2 in 8–14 μm, respectively. The specific radiant energy decreases by 43.2% in full wavelength after modified and the radiant power maximally reduce 72.5%. Above all, compare with the as-prepared CNP, the SMCNP broaden the absorption wavelength of the infrared spectra, especially in the range of 3–5 μm indicating the silver particles have significant contribution to increase the property. Considering the engineering application, this modified material was integrated with engineering matrix material, using glassfiber prepreg as an example, and still showed excellent energy saving results. Therefore, the SMCNP is a progressive candidate for infrared stealth application.

© 2015 Elsevier Ltd. All rights reserved.

1. Introduction

Infrared stealth is an indispensable technique in the modern detection industry and it has become a major focus with increasing demands for advanced detection and stealth technology. Generally, objects were exposed easily under the infrared detectors due to the high emissivity. In order to achieve infrared stealth camouflage, the infrared emissivity intensity discrepancy between the background and target object should be close enough that it is negligible for detection [1]. Nevertheless, the radiation intensity of most objects is higher than the background. The objects were invisible to infrared detectors under the protection of materials with low emissivity. Therefore, various materials with low emissivity, such as conductive polymeric materials [2], metallic powder composite [3,4], inorganic/organic composite [5] and semi-conductive materials [6], and manufacture processes have been reported in many literature. However, metallic powder was easily exposed to visible light due to the reflection of the metallic feature and was easy to be oxidized in long-term use, which leads to decrease the infrared stealth performance. Above all, the metallic film easily increases the total weight of the materials which is the most important problem in aerospace vehicles. Moreover, the conductive polymer and inorganic/organic composite coating were limited due to the poor infrared stealth performance, mechanical property and the complex binder manufacturing process [7]. Instead, advanced infrared stealth materials are required to be lightweight, thin and possess a broad wavelength band [8–10]. As the fiber reinforced polymer composite (FRP) developed gradually, the use of the FRP composite has significance in the modern aircrafts. Due to the FRP composites are manufactured by hot pressing or resin transfer molding (RTM), the metallic additive composite and inorganic/organic coating are different to achieve by integrally forming. In addition, metallic additive has a bad interface compatibility with the resin of FRP composite. Therefore, the typical infrared stealth methods, low-emissivity coating, metallic film and conductivity polymer, are not suitable for FRP composite. In this study, a silver particle modified carbon nanotube paper (SMCNP) infrared stealth material with lightweight, thin and broad wavelength band properties was proposed, which can be fabricated in an integral manufacture forming process.

* Corresponding author.
E-mail address: lengjs@hit.edu.cn (J. Leng).

http://dx.doi.org/10.1016/j.carbon.2015.11.036
0008-6223/© 2015 Elsevier Ltd. All rights reserved.

Carbon nanotube (CNT) remains one of the most attractive and well-studied materials systems in the scientific community due to its amazing variety and versatility in combine with easy preparation, availability, and wide ranging properties such as the infrared stealth [11–13], thermal [14], electronic [15,16], mechanical [17–19], optical properties [20–22] based on its structure, morphology and modified strategies. In most recent years, the study of carbon CNP has expanded into many areas from sensor [23], electronic devices [24], electrochemical batteries [25,26], super capacitors [27], flexible electronic [28], deicing composite [29] to energy harvester [30]. CNP is a porous assembly of CNTs, usually fabricated by filtration from their dispersion in a solvent [31–33], CNT forest [31,34] and the floating catalyst chemical vapor deposition. Moreover, due to the high electrical conductivity, thermal conductivity and mobility [35], CNP has been extensively used for sensing, photovoltaic and storage application.

CNT has been used as an additive in the infrared stealth coating materials [11–13,36–40]. In this paper, an integral manufacture forming process of an ultra-low infrared emissivity material of SMCNP/glassfiber reinforced polymer (GFRP) composite for infrared stealth was developed successfully. To broaden and increase the absorption of the infrared wavelength band, a little amount guest material, silver nano-particles, was introduced to the hosted CNP which was achieved by absorbing silver nitrate aqueous. The silver nitrate was decomposed as guest silver particles on the CNP surface when it was exposed in the fluorescent lamp. In terms of the previous reports [41–44], for film material, infrared emissivity is associated with the sheet resistance (SR). Therefore, the sheet resistance is a key parameter for low infrared emissivity material. After introducing the guest component, the SR was reduced by more than 92.9%. The infrared emissivity decreases dramatically of the atmospheric window wavelength, 3–5 μm and 8–14 μm, maximum 38.9% and 55.7%, respectively, especially in 3–5 μm performing much better than the as-prepared CNP. In the full-wavelength test, the infrared emissivity presents SMCNP and SMCNP/GFRP composite is below 0.65 much lower than CNP performance. The maximum radiant energy decreases by 43.2%. Therefore, the SMCNP is a promising candidate in the future infrared stealthy technique for the FRP composite structure.

2. Experimental section

2.1. Materials

SWCNT were purchased from Chengdu Organic Chemicals Co. Ltd., Chinese Academy of Sciences and used without further purification. The average diameter and lengths of the individual tube are 3–5 nm and 5–30 μm respectively synthesized by a chemical vapor deposition with carbon content more than 90wt%. Commercially available polyoxyethylene octylphenylether, biochemical grade, was obtained from Aladdin Chemical Reagents Co., Ltd., China employed as a non-ionic surfactant to prevent aggregation of the SWCNT. Silver nitrate was provided by Aldrich and used as received. Glassfiber presoak used in this study was purchased from ShangWei Wind Power Material Co., Ltd., China.

2.2. Measurements

Conductivity was measured using a Napson Resistivity Measurement System (RG-7C) Four Point Probe with 0.4 mm probe diameter and 1.0 mm tip spacing. The load on the probe was 50 g.

The Roman spectra were recorded using an Almega-Dispersive Raman (Thermo Nicolet) with 532 nm excitation.

Thermal gravity analysis (TGA) was performed with a Mettler Toledo TGA/DSC1 instrument at a heating rate of 10 °C/min from 25 to 1000 °C in air atmosphere Scanning electron microscopy (SEM) observations were characterized using a Quanta 200 F Field-Emission Scanning Electron Microscope (FE-SEM) with an operating voltage of 30 kV. Atomic Force microscope (AFM) image were achieved by Bruker Multimode 8 with the ScanAsyst in air experiment method.

The contact angle test was carried out using a microscopic Contact Angle Measurement (OCA20, GFR), at room temperature. The characterization was used to demonstrate the resin spread capacity on the CNP surface.

Infrared radiant property of composite and CNP was detected by an infrared temperature camera (VarioCAM HiRes sl, JENOPTIK Infra Tec) with recognizable wavelength ranging from 8 to 14 μm.

Nitrogen adsorption isotherm measurement was analyzed by a Micrometrics ASAP 2020 volumetric adsorption analyzer at 77 K using Barrett-Emmett-Teller (BET) to calculate the specific surface area. The pore size distribution was illustrated on the adsorption branch of the isotherm using density functional theory (DFT) model.

Mechanical properties of the CNP were studied using a Zwick/roll Materials Testing Machine with a 100 N load cell, following the mounting specification indicated by ASTM standard D638 TypeVI. The crosshead speed applied was 2 mm/min. At least 5 dumbbell samples prepared by laser cutting machine were tested and selected three of the results were averaged.

Continuous wavelength infrared emissivity at different temperature is performed by CI System SR-5000 N Spectroradiometer.

The mixture of SWCNT and surfactant was dispersed by three roll shearing disperser (DS50, EXAKT).

2.3. Methods

2.3.1. Fabrication of self-assembly hosted CNP

To fabricate the self-assembly CNP, typically, 0.25~1 g SWCNT were mixed with 1~4 g Triton X-100. To fully mix the SWCNT with surfactant, the mixture was dispersed by shearing disperser to form a pasty hybrid compound. Subsequently, the pasty mixture was diluted in 5 L deionized water and dispersed using a ultrasonic processor as our previous report [29].Then, the CNT solution was filtered through a porous membrane to form the as-prepared CNP. The CNP was peeled off the membrane after drying treatment at 90 °C for 2 h. The thickness of the hosted CNP was controlled by the concentration of CNT solution with three kinds of samples, 67 μm, 130 μm and 200 μm, which were used in this study. The as-prepared CNP was treated under 380 °C according to the TGA results (Fig. S1) for 2 h in a muffle furnace to remove the Triton. Then the different thickness samples were cut into circular sheets with the diameter of 4 cm.

2.3.2. Preparation of silver particles modified CNP

The silver nitrate aqueous solution with the concentrations of 0.1 ml/L, 0.3 mol/L and 0.5 mol/L was prepared in the deionized water without exposing the light during the processes. CNP circular sheets were immersed into the silver nitrate aqueous solution for 5 h. Because of large surface area of the CNT, silver and nitrate ions adsorb gradually on the surface of hosted CNP until reach the adsorption equilibrium. Subsequently the sheets were dried under 50 °C for 3 h to remove the deionized water. As we know, when silver nitrate is exposed under the light, it decomposes into silver, nitrogen dioxide and oxygen as shown in Scheme 1. Dried CNPs

$$2AgNO_3 \xrightarrow{\text{light}} 2Ag + 2NO_2\uparrow + O_2\uparrow$$

Scheme 1. The photolytic equation of the silver nitrate exposed in light.

were irradiated under a fluorescent lamp for 4 h to form the silver particles.

2.3.3. Fabrication of the Glassfiber/SMCNP (SMCNP/GFRP)

SMCNP/GFRP composite was prepared by vacuumed hot pressing method and the layout is shown in Fig. S2a. The size of the GFRP laminate was 100 × 100 × 2 mm^3 with orthogonal ply between each layer. The SMCNP was laid out on the surface of GFRP prepreg. Then the composite was vacuumed to 10^{-3} Pa in the autoclave under 0.4 Mpa of the outside pressure with the heating process treatment as indicated in Fig. S2b. The fabricated schematic diagram of the SMCNP/GFRP composite in an integral forming process was shown in Fig. 1.

3. Results and discussion

3.1. Self-assembly CNP fabrication and morphology characterization

The detailed fabrication procedures of CNP were described in the previous report [29]. The gross visual appearance of the as-prepared CNP is demonstrated in Fig. 2a with the size of 265 × 180 × (0.067/0.13/0.2) mm^3. It is obvious that the CNP is smooth as the copy paper. The insert picture is the surface morphology change of the as-prepared CNP before and after folding by a minimal radius of curvature. After unfolding the CNP, the surface of the CNP wasn't damaged in the crease line, which shows that the CNP possesses high flexibility compared with the previous works [45–47]. This property ensures the hosted CNP can be manipulated in the vacuumed hot-forming process. The FE-SEM image of the as-prepared CNP before heating treatment is shown in Fig. 2b. Obviously, a random network is formed between CNTs and large amounts of physical crosslinked points are achieved due to the electrostatic force, which is in favor of electronic conduction. Insert red rectangle is the partial enlarged image, it is clear that amorphous particles distribute in the pores of CNT networks and the surfaces are a bit rough distinguishing from the bright reflection. This is caused by the agglomeration and residual surfactant wrapping up the CNTs. The morphology of the CNP after heat treatment at 380 °C is demonstrated in Fig. 2c. It reveals homogeneous CNP is obtained by the self-assembly processing. The Raman spectroscopy of the CNTs and the heat treated CNP is shown in Fig. S3. The ration of D/G band intensity has a small increase from 0.023 to 0.036 indicating that the ultrasonic caused week defects on the CNTs. Compared with Fig. 2b, the smooth surfaces indicate the residue surfactant is removed entirely under the heat treatment and the blocked holes between the tubes are open. Subsequently, the treated CNP was immersed in silver nitrate aqueous for 5 h until the adsorption equilibrium. The CNP after the photolysis was shown in Fig. 2d. As displayed in the image, uniform size silver particles deposit discretely around CNT bundles and also fill in the void space in the network indicating the high affinity of the silver nanoparticles to the CNT frameworks. From the insert enlarged image, silver particle diameter is around 100 nm.

Therefore, this is a facile and helpful strategy to deposit tiny amount silver particles on various substrates. Compared with the commonly used methods such as electrochemical deposition [48–51], a remarkable advantage is immersed method can be used for preparing large scale particle modified material which is a significant factor for engineering application. The crystal structure was measured by XRD as shown in Fig. 2d. It indicates that the silver nitrate has decomposed after exposing in the light for a period of time. The corresponding lattice planes are marked on the curve, which is detected by contrasting the phase with standard data.

3.2. Pore structure and polymer compatibility

As an engineering application, SMCNP need to cover on FRP surface such as GFRP prepreg or carbon fiber reinforced polymer (CFRP) composite. Therefore, it is a key perimeter to investigate the interface compatibility between polymer and CNP. To present the porous structure of the CNP, the high-resolution AFM image of the CNP after heat treatment is presented in Fig. 3a. The random CNTs formed a high porous film, meaning that resin is able to infiltrate into these pores to enhance the interface feature between resin and CNP. The inner blue curve is the height variation in the z axis of the white arrow presenting that a hierarchical porous morphology was self-assembly successfully. Moreover, the pore diameter distribution curve (Fig. 3b) achieved by BET further confirms that the CNP is porosity structure. Two peaks at 2 nm and 25 nm exhibit the main pores belong to the mesoporous range.

Additionally, pore diameter distributes in a wide range from 2 nm to 100 nm, indicating CNP has high pore volume fraction. The epoxy spreadability on the CNP was determined by contact angle test shown in Fig. 3b. The contact angle of the interface is 24.5° meaning that resin can spread on the surface easily. Fig. 3c is the polished cross section FE-SEM image of CNP/GFRP composite fabricated by vacuumed hot-pressing integral manufacture forming process. It is obvious that the interface of the CNP and resin is no crack and contact together closely on the boundary shown in the two red dash line rectangles. The similar contrast between the CNP layer and epoxy resin layer means that part of the epoxy has infiltrated into the CNP, and the top rectangle indicates a small amount resin permeates the CNP. Therefore, there is a good interface compatibility property between CNP and GFRP composite, which determines the feasibility of engineering manufacture process and the application.

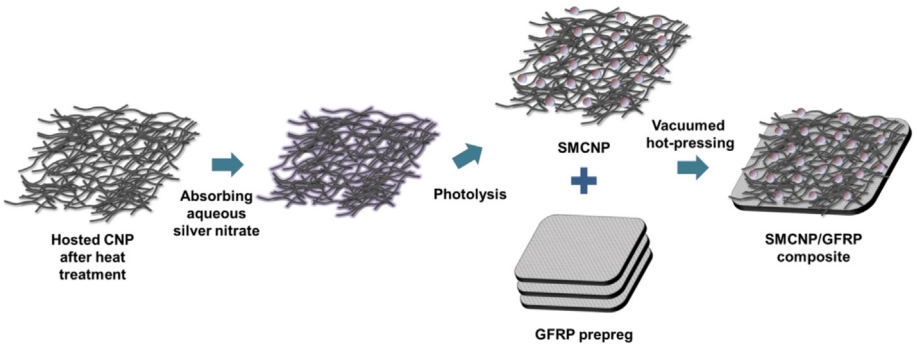

Fig. 1. Schematic diagram of the SMCNP/GFRP composite prepared by an integral manufacture forming process (A color version of this figure can be viewed online).

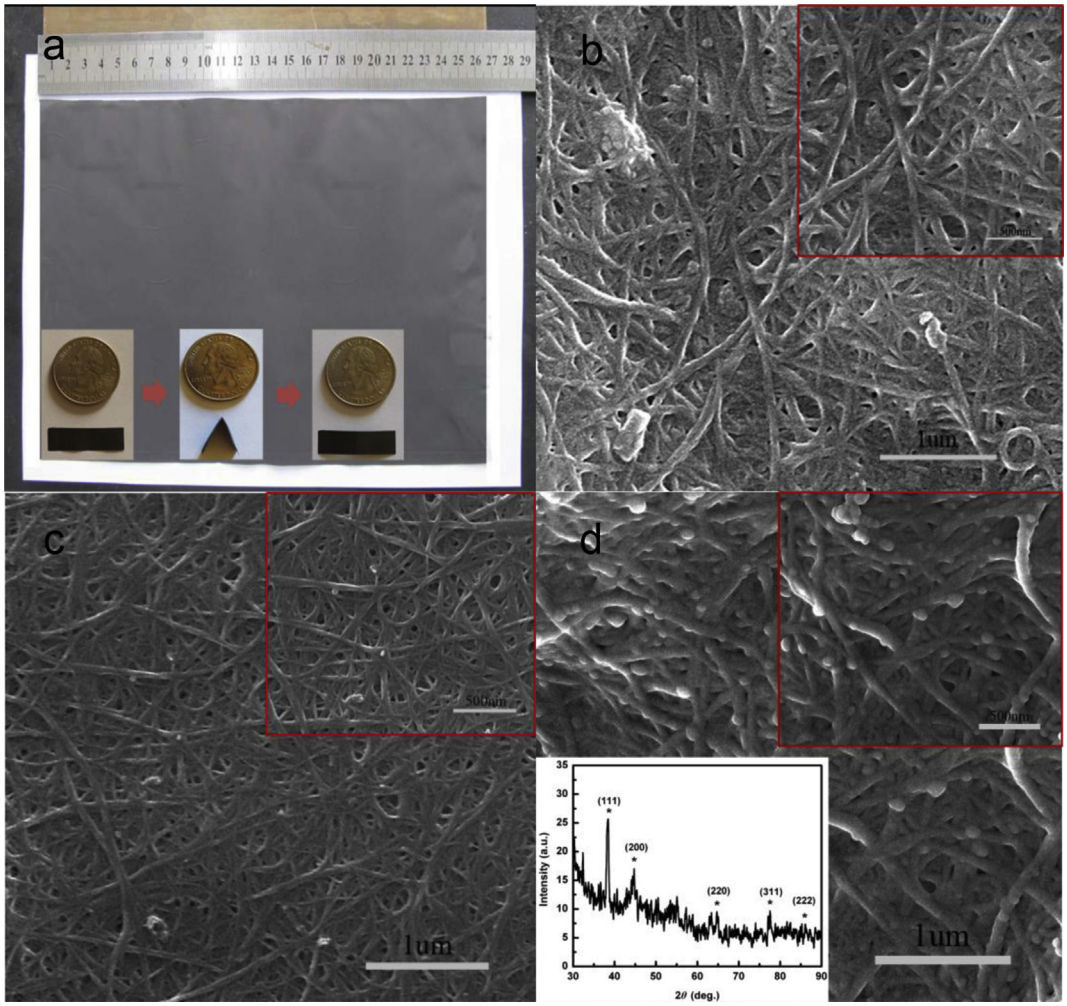

Fig. 2. Morphology of CNP and SMCNP. a) Digital photo of as-prepared CNP and the flexibility test. b) FE-SEM image of the as-prepared CNP. c) Morphology of the CNP after heating treatment. d) FE-SEM image of SMCNP after being modified and the inner curve is the Ag XRD deposited on the SMCNP surface (A color version of this figure can be viewed online).

3.3. Conductivity and mechanical properties

Conductivity and SR are the significant properties for low thermal radiant materials, due to the absorption of sub-bandgap IR light by free carriers gives a measure of the free carrier density, which is relevant to the SR value [41–44]. High SR value means possess higher infrared radiant ability, whereas the low SR implies the material has a lower infrared emissivity. Fig. 4a are the electrical conductivity results after various treatments. The sintered CNP has a modest increase, from 108 S/cm to 220 S/cm. Due to the surfactant is a poor conductor; the residual surfactant between tubes hinders the conduction of electrons. It is apparent, however, the conductivity rises sharply, from 220 S/cm to 1700 S/cm, after introducing a small amount of guest silver particles. The conductivity modified by 0.5 mol/L silver nitrate increases by 16 times compared with the as-prepared CNP, and over 50 times higher than the flexible graphite foils [52,53]. Based on the above discussion, in the FE-SEM image, the guest silver particles only discretely distribute on the surface of hosted CNP as shown in the schematic (Fig. 4b). Hence, why a small amount discrete guest silver particles can improve the conductivity significantly. According to the previous reports, for the bundled CNP, electric current only flow on the outer metallic tubes of a bundle, while the inner tubes do not contribute significantly to the current [54]. As shown in Fig. 4b, the electrons mostly conduct on the outer metallic CNTs of the bundles; therefore the outer layer is the main factor influencing the electrical conductivity while the inner metallic and semiconducting tubers can be negligible. For the outer tubes, the silver particles deposit around the tubes and also in the void space. In this case, the contact points between nanotubes are equivalent to a resistor [54] as illustrated in the enlarged schematic diagram of Fig. 4b and the inserted silver particle shorts out the three contact resistors due to the intrinsic great electrical conductivity. Therefore, silver particles on the surface imply to short out a lot of resistors resulting in the sharp improvement of conductivity, although just a small amount and discontinuous silver particles. As silver nitrate concentration increased, the SR decreases dramatically from 700 to 50 mΩ/sq and reach an approximate constant value at the 0.5 mol/L. In view of the proportional relationship between infrared emissivity and SR, it should be concerned to reduce the SR for the low infrared emissivity materials.

The silver amount of the modified hosted CNPs by different concentration solution was measured by the TGA in air atmosphere from room temperature to 1000 °C as displayed in Fig. 4c and the residual amount are listed in Table 1. The residual component is the oxidizing catalyst using for growing CNTs of the blank sample. However, the SMCNP has many weight loss steps demonstrated in the other three curves which are attributed to silver nitrate

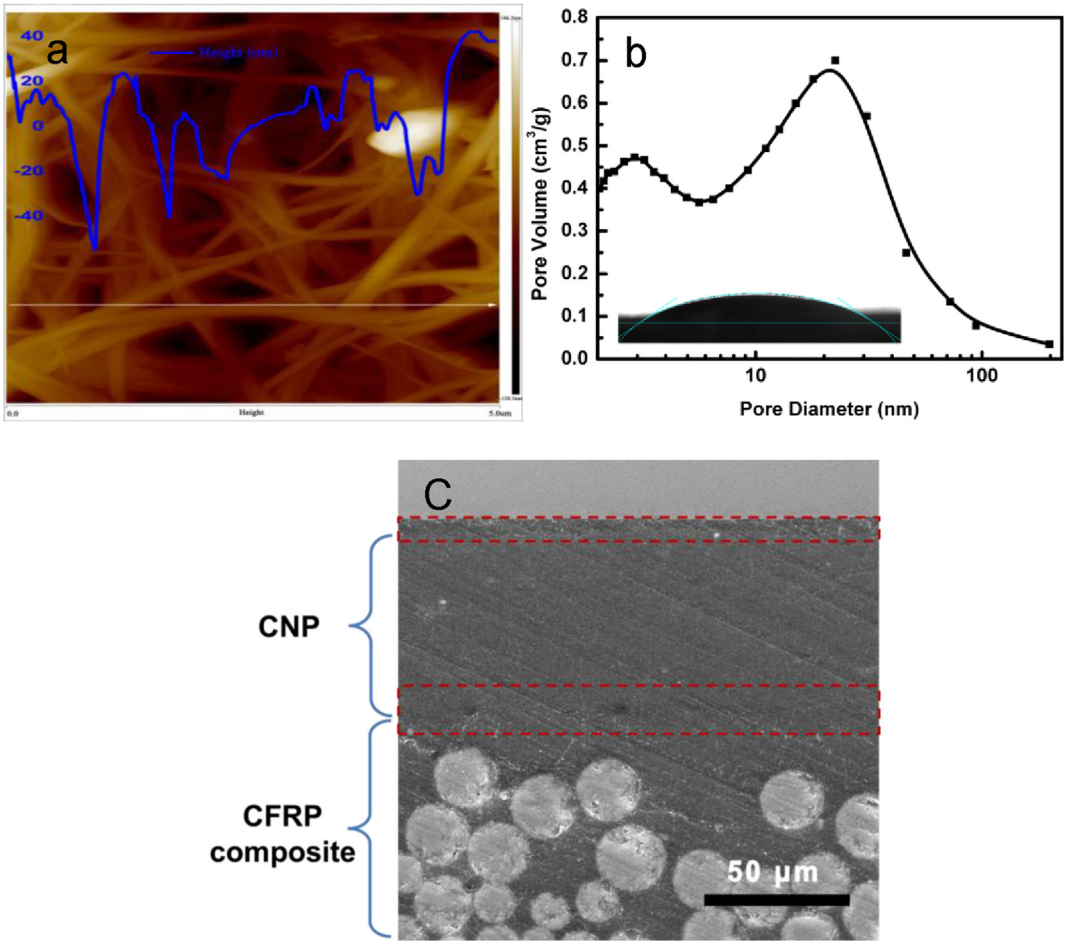

Fig. 3. a) AFM phase image of the CNP after heating treatment, the blue curve is the height change of the z axis on the white arrow. b) The pore diameter distribution of the CNP and the interface, contact angle test for displaying the spreadability of epoxy on CNP. c) The cross section FE-SEM picture of CNP/GFRP composite (A color version of this figure can be viewed online).

decomposition. By increasing the solution concentration, the silver amount rises gradually according to the residual values as shown in Table 1.

Mechanical property was tested by a Zwick/roll Materials Testing Machine using dumbbell samples. As presented in Fig. 4d, the rupture stress and strain of the as-prepared CNP is about 16 MPa and 2.25%, respectively lower than the heating treated and SMCNP samples. The reason causing the mechanical decrease is the surfactant cover on the CNT's surface, preventing the interaction between CNTs resulting in a lower strain, because surfactants play a role of lubrication. Additionally, Triton is a liquid chemical at room temperature and it should slide when the molecule suffers a shear force between CNTs under the tensile stress; therefore it is a nature the slide easily reduces the breaking stress. Comparing the heat-treated and SMCNP samples, breaking stress and strain has a little change around 25 MPa and 3.5%, respectively, indicating that the guest silver particles maintain the original mechanical structure after the modification, which ensures that the maneuverability of the later integrated process.

3.4. Infrared emissivity

Thermal radiant properties of the SMCNP are studied by the infrared emissivity which is a significant parameter for low thermal radiant materials. The low thermal radiant material is a kind of insulating materials by reflecting the infrared. The performance of reflective insulation depends on many factors such as emissivity of the material, temperature gradient on both sides of the reflective material and the direction of heat flow. The following Eq. (1) can describe the energy reaction approach for materials where α means the absorbed fraction of incident radiation through the material; τ means the transmitted fraction of incident radiation through the material; ρ means the reflected fraction of incident radiation of the material. Based on the Kirchhoff's radiant law, at the temperature equilibrium, the emissivity and reflectivity are a proportional relation of any kind of materials. Therefore, it is reasonable that the infrared stealth performance can be characterized by testing the emissivity.

$$\alpha + \tau + \rho = 1 \tag{1}$$

The SMCNP was cut as a circular sample with the diameter of 4 cm as shown in Fig. 5a and was integrated with glassfiber prepreg by vacuum hot-pressing to form the SMCNP/GFRP composite as presented in Fig. 5b.

The infrared emissivity was characterized by an infrared camera and schematic diagram of the test system as shown in Fig. S4. SMCNP samples were heated on the heating plate to a balanced temperature. Infrared camera detected the temperature discrepancy between the background and the samples to calculate the infrared emissivity of samples. Furthermore, considering the engineering application, the SMCNP/GFRP composite samples were

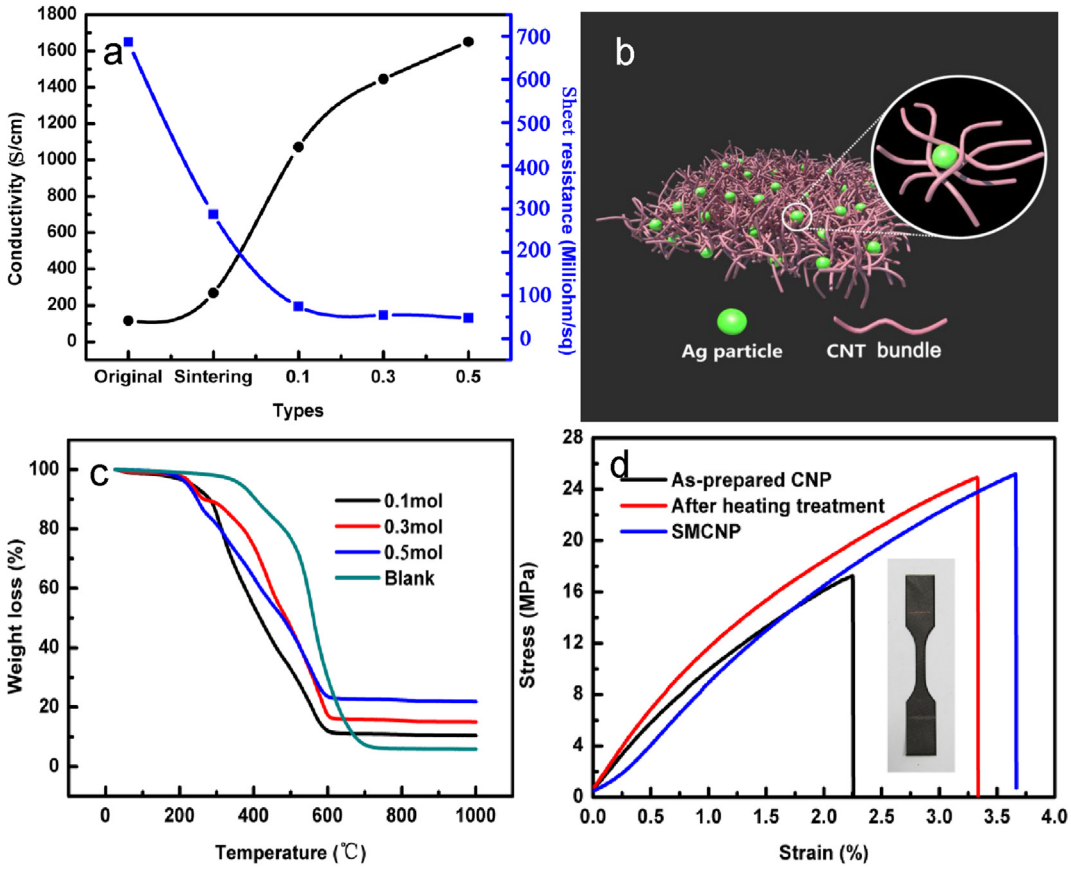

Fig. 4. a) Conductivity and SR test of different types of CNP and SMCNP. b) Schematic diagram of the modified SMCNP. c) TGA test of SMCNP modified by different solution concentration. d) Mechanical property of different kinds of CNP and the dumbbell shape sample using in this experiment (A color version of this figure can be viewed online).

Table 1
Residual amount and Ag mass fraction of different modified samples.

	Blank	0.1 mol/L	0.3 mol/L	0.5 mol/L
Residual amount (wt%)	5.9	10.5	15.1	21.9
Catalyst (wt%)	5.9	5.7	5.4	5.2
Ag amount (wt%)	0	4.8	9.7	16.7
Atomic ration (C:Ag)	0	168:1	79:1	42:1

fabricated to simulate the composite component of an aircraft structure. Therefore, it is essential to study the infrared emissivity variation after being integrated manufacture forming process. Fig. 5c is the 2D and 3D temperature field distribution identified via color change after the heater temperature balancing at 223 °C with three round samples modified by different concentration of silver nitrate solution. In the 3D thermography, it is clear to realize the temperature field distribution. The line temperature distribution of the triangle drawn in the 2D thermography is presented in Fig. 5c.The start point is the ambient temperature and the pink surface is the heating plate area. From the curve, it is obvious that the temperatures of ambient and heating plate are about 33 °C and 223 °C, respectively. However, when the line crosses the samples, it drops sharply close to 80 °C–95 °C. The average temperatures of the three round samples are 92.15 °C, 85.64 °C and 79.56 °C, respectively, as the concentration increased meaning that guest silver particles enhance the infrared stealth performance. It indicates the SMCNPs radiate much less energy than the heating plate background. In terms of the Kirchhoff's radiant law, the SMCNPs have a low infrared emissivity and are able to decrease the SMCNP temperature to ambient temperature, which camouflages the target object. The supplementary movie 1 is the dynamic equilibrium radiant process of the SMCNP modified by different concentration aqueous at 150 °C. The supplementary movie 2 is an odd sample modified by 0.3 mol/L silver nitrate aqueous in a oven. Afterward, the oven lid was opened quickly, when the oven reached an equilibrium temperature measured by a thermocouple. The infrared camera recorded the dynamic radiant process. The boundary of the odd shape (blue area) is clearly distinguished from the movie indicating there is a big temperature discrepancy between the sample and the background. The dynamic line temperature change of the odd sample after opening the lid is shown in Fig. S5. The infrared emissivity of the as-prepared CNP with different thickness was studied at various temperatures from room temperature to 230 °C (Fig. 5d) with the infrared wavelength between 8 and 14 μm. As the thickness increased, the infrared emissivity decreases a little while the temperature over 160 °C, the infrared emissivity of different samples has a small discrepancy which demonstrates sample thickness has a weak effect on the infrared emissivity.

Supplementary video related to this article can be found at http://dx.doi.org/10.1016/j.carbon.2015.11.036.

Fig. 5e is the surface temperature of the different SMCNPs at various plate temperatures. As can be seen in the curves, sample temperatures are much lower than the heating plate temperatures because the SMCNP has a weaker infrared emissivity than the heating plate. Moreover, the sample modified by higher concentration shows lower surface temperature than the as-prepared CNP, such as decreasing by more than 30 °C between the as-prepared

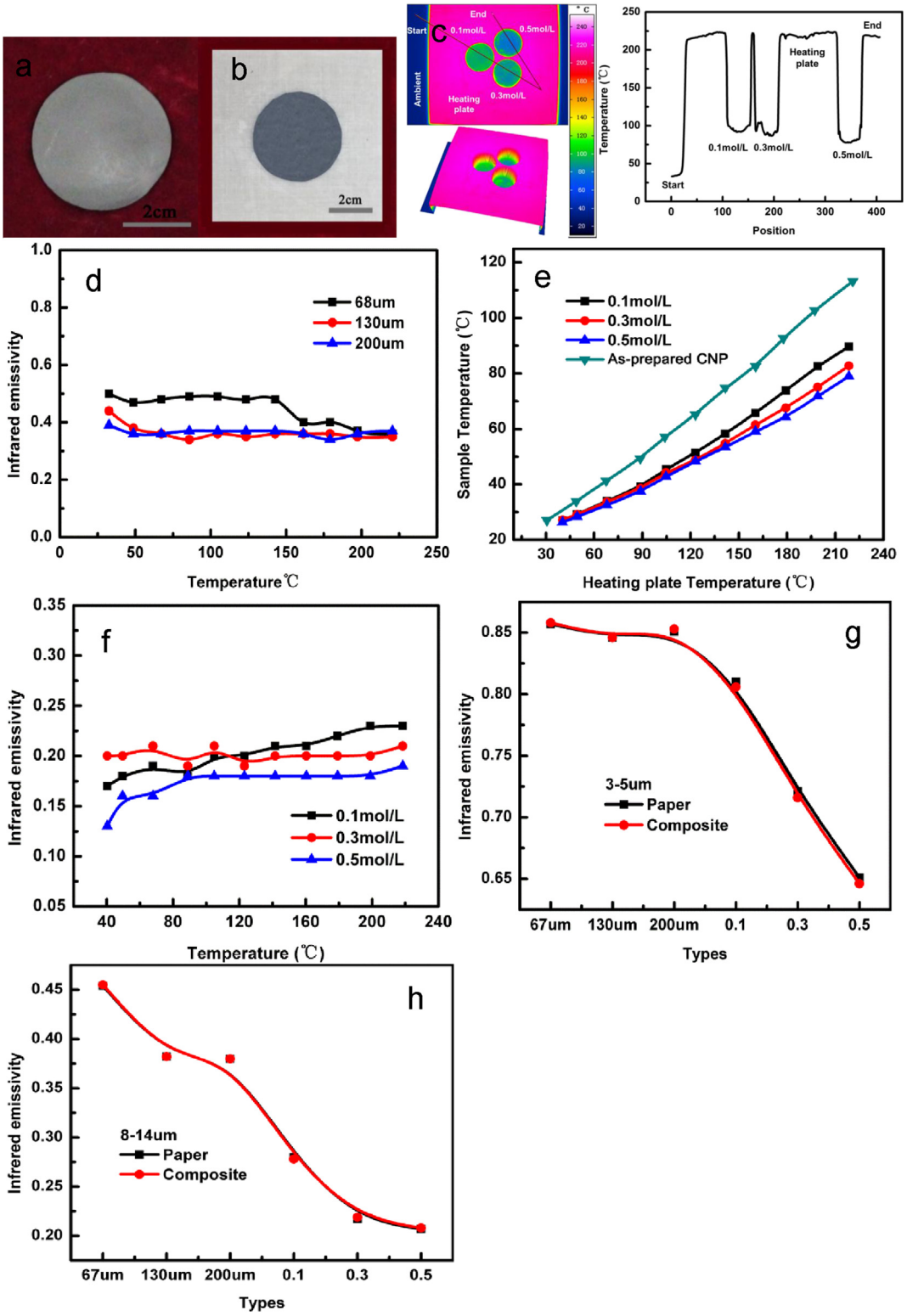

Fig. 5. a) Image of SMCNP sample for infrared emissivity test. b) Image of SMCNP/GFRP composite sample prepared by the integral manufacture processing. c) 2D and 3D thermography of the heating plate and SMCNP modified by different solution concentration and line temperature field distribution of the triangle on the thermography is shown in the right figure d) Comparison sample temperature data of different types of CNP at different heating plate temperature. e) Variable temperature infrared emissivity of the different thickness CNP samples. f) Variable temperature infrared emissivity of the different SMCNP sample. The infrared emissivity of different thickness and various SMCNP samples modified by 0.1 mol/L, 0.3 mol/L and 0.5 mol/L silver nitrate solution of g) the CNP/SMCNP and corresponding composite at 3–5 μm; h) the CNP/SMCNP and corresponding composite at 8–14 μm (A color version of this figure can be viewed online).

CNP and 0.5 mol/L SMCNP at 230 °C, which suggests the amount of the guest silver particles on the hosted CNP surface is helpful to

reduce the infrared emissivity. In order to study the guest silver particles amount effect on infrared emissivity at varying temperatures, the infrared emissivity of SMCNPs modified by different concentration is shown in Fig. 5f. Small fluctuation is achieved as the temperature increase in a wide range which demonstrates the SMCNP has a stable infrared emissivity even though in a high temperature. According to the above analysis, the optimized SMCNP thickness is 130 μm and the proper silver nitrate concentration is 0.5 mol/L, which are used as the optimal prepared conditions.

Given the engineering application, the SMCNP should be manufactured with other FRP composite. In this case, SMCNP/GFRP composite was prepared by vacuum hot-pressing manufacture. Fig. 5g and h are the comparison infrared emissivity results of SMCNP and SMCNP/GFRP composite at room temperature under different infrared wavelengths because wavelengths between 3 and 5 μm and 8–14 μm are the atmospheric infrared window which is the main investigated bands in the infrared stealth. Therefore, the emissivity of the both wavelengths is the key parameter that determines infrared camouflage performance. Based on Fig. 5g, as the thickness of the as-prepared CNP increase, the infrared emissivity is almost the same varying around 0.85 while the emissivity decreases to 0.65 as modified solution concentration increased, from 0.1 mol/L to 0.5 mol/L. The infrared emissivity shows that the as-prepared CNP has weak infrared stealth performance in 3–5 μm wavelength while the performance improves dramatically after introduce the guest silver particles because of the synergistic effect between CNTs and the silver particles. For the 8–14 μm, the infrared stealth performance also improves gradually as the modified concentration increased and reach a constant emissivity around 0.2 at 0.3 mol/L and 0.5 mol/L which means the SMCNP has an excellent infrared insulating property. From the both figures, the infrared emissivity of SMCNP decreases by 38.9% and 55.6%, respectively of the both wavelengths. The performance is much better than the previous reported non-metallic materials which are compared in Table 2. In the both wavelength ranges, 3–5 μm and 8–14 μm, the emissivity of this work decreases sharply than the previous work.

3.5. Variable temperature full-wavelength infrared emissivity and radiant energy

In terms of the practical application, it is essential to investigate the infrared stealth property of the composite material after manufacture and the valid operating temperature range. Therefore, the full-wavelength infrared emissivity of the CNP/GFRP composite and SMCNP/GFRP composite results at various temperatures are demonstrated in Fig. 6a. It is obvious that the SMCNP/GFRP composite samples have a much lower emissivity than CNP/GFRP composite, especially in the short wavelength below 4 μm exhibiting a sharp decrease from ~1 to ~0.6 at low temperature. The result presents the guest silver particles not only enhances the infrared stealth in the wavelengths of 3–5 μm and 8–14 μm but also improves the performance to the full wavelength.

In the full wavelength, the SMCNP/GFRP infrared emissivity is lower than the CNP/GFRP composite as the wavelength increasing. The performance presents the guest silver particles provide positive effects for infrared stealth in the short wavelength and enhance the camouflage property in the full wavelength. To test the operating temperature range, the composite was carried out at various temperatures as high as the GFRP available. Below 300 °C, SMCNP/GFRP composite emissivity is much lower than CNP/GFRP composite and has a tiny variation at different temperatures. Based on the above test, it is can also support the guest silver particle contribute to the infrared stealth in the host-guest material. Obviously, the infrared emissivity of SMCNP/GFRP composite is below 0.65 in the full wavelength from 100 °C to 400 °C (resin decomposition temperature) meaning that SMCNP is a progressive candidate as an infrared camouflage material at the high background temperature, which can be used in the high temperature components of an aircraft. High operating temperature, full-wavelength performance, stable property and integrally forming process indicate SMCNP/GFRP composite is suitable for the advanced FRP engineering application. According to Plank's law, the relationship between emissivity and electromagnetic wavelength is shown in Eq. (2) where $I(\lambda, T)$ is the emissivity; h is the Plank constant and; c is the light speed in the medium; κ is the Boltzmann constant; λ is the wavelength of the electromagnetic and T is the absolute temperature.

$$\mathrm{I}(\lambda,\mathrm{T}) = \frac{2hc^2}{\lambda^5}\frac{1}{e^{\frac{hc}{kT\lambda}}-1} \tag{2}$$

$$\mu(\lambda,\mathrm{T}) = \frac{4\pi}{C} I(\lambda,T) \tag{3}$$

From the Eq. (3), the energy density is proportional to emissivity by multiplying $4\pi/c$. Therefore, when the absolute temperature is a constant, the area under the curves of Fig. 6a corresponds to the radiant energy in the full wavelength. In that case, the integral area is presented in Fig. 6b. The column chart is the relative radiant energy of the CNP/GFRP and SMCNP/GFRP composite at different background temperatures. As described in the figure, the SMCNP/GFRP composite radiate less energy than the CNP/GFRP composite especially below 300 °C. Compared to the GNP/GFRP, the radiant energy of SMCNP/GFRP decreases from 43.2% to 8.3% as the temperature increased.

3.6. Radiated power

To calculate the infrared stealth performance of CNP and SMCNP, the radiated power of the background (bare heating plate), CNP and SMCNP covered plate was detected by infrared camera from room temperature to 230 °C for the 8–14 μm wavelength. Fig. 7a is the comparative data covered different thickness CNP. It is clear that CNP samples have a smaller slope than the bare heating plate. The

Table 2
The compared infrared emissivity of this work with the previous reports.

Materials	Infrared emissivity	Wavelength range (μm)	References
SiO_2 film	0.87	2–22	[55]
SiO_2@Bi_2O_3 composite	0.75–0.82	2–22	
W-doped VO_2 film coating	0.75–0.95	8–14	[56]
ZnO: (Al, La) particles	0.62–0.79	8–14	[57]
Ni–P modified hollow cenosphere	0.6–0.9	8–14	[58]
This work	0.20–0.26	8–14	–
SMCNP or SMCNP/GFRP composite	0.64–0.8	3–5	

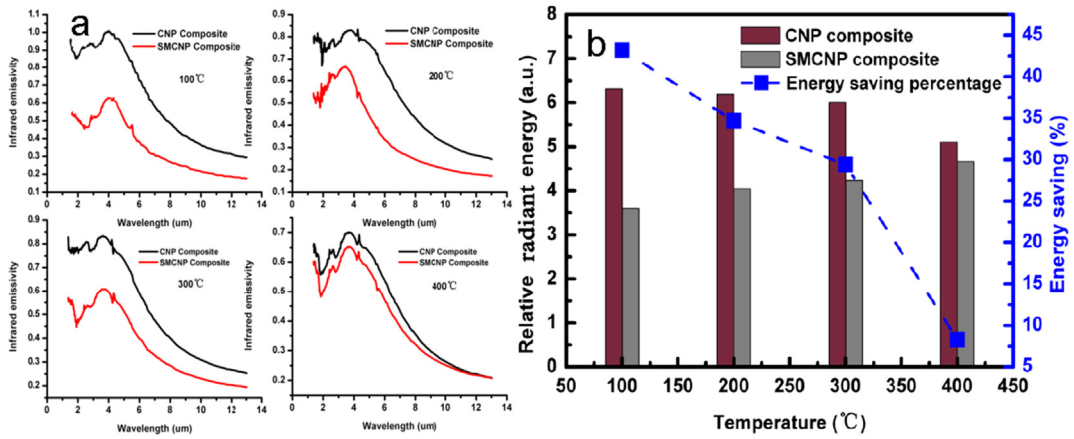

Fig. 6. a) Variable temperature full-wavelength infrared emissivity test of CNP/GFRP and SMCNP/GFRP composite. b) The relative radiant energy of CNP/GFRP composite and the energy saving curve of SMCNP/GFRP composite (A color version of this figure can be viewed online).

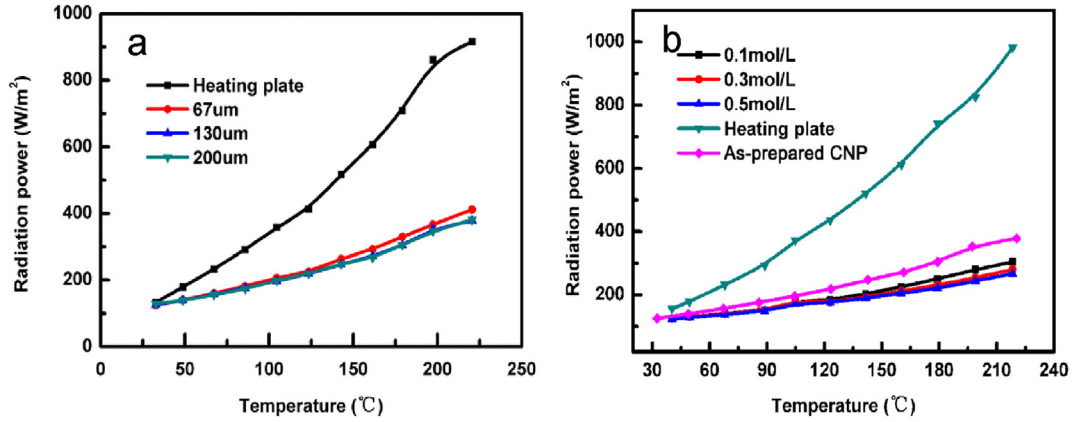

Fig. 7. a) Comparison radiant power of different thickness CNP samples and bare heating plate. b) Comparison radiant power between the different CNP and SMCNP with 130 μm and bare heating plate (A color version of this figure can be viewed online).

radiation power decreases more than 50% in 230 °C.

Compared the different thickness samples, the radiant power has tiny change at each temperature, meaning that the thickness has little effect on infrared emissivity. Fig. 6b compares different samples with the same thickness. After modified, SMCNP further drops the radiant power than the as-prepared sample. At 230 °C, the radiant power reduces by 72.5% between the bare heating plate and 0.5 mol/L samples while the two curves are almost overlap of the samples modified by 0.3 and 0.5 mol/L silver nitrate, which demonstrates that 0.3 mol/L is sufficient for the modified solution concentration to achieve a great infrared camouflage performance.

4. Conclusions

A SMCNP and integrally manufacture forming process SMCNP/GFRP infrared stealth composite materials were prepared successfully based on CNP. The conductivity of the porous CNP increases by 673% from 220 S/cm to 1700 S/cm with the silver mass of 16.7 wt%. The mechanical property increases from 16 MPa to 24 Mpa after heating treatment. For the SMCNP/GFRP composite, in 3–5 μm and 8–14 μm, the infrared emissivity decreases dramatically, maximum 38.9% and 55.7%, respectively, especially in 3–5 μm wavelength band. Variable temperature full-wavelength test indicates that SMCNP/GFRP composite infrared emissivity is below 0.65 from 100 °C to 400 °C much lower than CNP/GFRP composite. Additionally, the maximum radiant energy saving reaches to 43.2% and the maximum radiated power reduces by 72.5%. High operating temperature, full-wavelength performance, stable property and integrally forming process indicate SMCNP/GFRP composite is a candidate for the advanced FRP engineering camouflage material in aerospace area.

Acknowledgments

This work is supported by the National Natural Science Foundation of China (Grant No.11225211, No.11272106).

Appendix A. Supplementary data

Supplementary data related to this article can be found at http://dx.doi.org/10.1016/j.carbon.2015.11.036.

References

[1] T. Hallberg, T. Niinimäki-Heikkilä, E. Hedborg-Karlsson, P.S. Salonen, C. Nilsson, A. Jänis, Development of Low-emissive Camouflage Paint: Final Report: Sensor Technology, Swedish Defence Research Agency, 2005.
[2] W. Zhang, G. Xu, R. Ding, K. Duan, J. Qiao, Nacre biomimetic design—a possible approach to prepare low infrared emissivity composite coatings, Mater. Sci. Eng. C 33 (1) (2013) 99–102.
[3] C.R. Sutter, R.A. Petelinkar, R.E. Reeves, Infrared Reflective Visually Colored Metallic Compositions, Google Patents, 2002.

[4] H. Yu, G. Xu, X. Shen, X. Yan, C. Cheng, Low infrared emissivity of polyurethane/Cu composite coatings, Appl. Surf. Sci. 255 (12) (2009) 6077–6081.
[5] C. Yang, Y. Gung, W. Hung, T. Ting, K. Wu, Infrared and microwave absorbing properties of $BaTiO_3$/polyaniline and $BaFe_{12}O_{19}$/polyaniline composites, Compos. Sci. Technol. 70 (3) (2010) 466–471.
[6] P.K. Biswas, A. De, N. Pramanik, P. Chakraborty, K. Ortner, V. Hock, et al., Effects of tin on IR reflectivity, thermal emissivity, Hall mobility and plasma wavelength of sol–gel indium tin oxide films on glass, Mater. Lett. 57 (15) (2003) 2326–2332.
[7] L. Yuan, X. Weng, L. Deng, Influence of binder viscosity on the control of infrared emissivity in low emissivity coating, Infrared Phys. Technol. 56 (2013) 25–29.
[8] B. Yu, L. Qi, Ye Jz, H. Sun, Preparation and radar wave absorbing characterization of bicomponent fibers with infrared camouflage, J. Appl. Polym. Sci. 104 (4) (2007) 2180–2186.
[9] J. Zhou, J. He, G. Li, T. Wang, D. Sun, X. Ding, et al., Direct Incorporation of Magnetic Constituents within Ordered Mesoporous Carbon– Silica Nanocomposites for Highly Efficient Electromagnetic Wave Absorbers, J. Phys. Chem. C 114 (17) (2010) 7611–7617.
[10] L. Chen, C. Lu, Y. Lu, Z. Fang, Y. Ni, Z. Xu, Microwave absorption and infrared performance of $Sm_{0.5}Sr_{0.5}Co_{1-x}Ni_xO_3$ ($0 \le x \le 1.0$) with the K_2NiF_4 structure, RSC Adv. 3 (12) (2013) 3967–3972.
[11] X.S. Tang, Carbon Nanotube Coatings for Visible and Ir Camouflage, Google Patents, 2011.
[12] M.J. Jackson, D. Spooner, Camouflage Utilizing Nano-optical Arrays Embedded in Carbon Matrix, Google Patents, 2013.
[13] R.Z. Zhang, X. Liu, Z.M. Zhang, Modeling the Optical and Radiative Properties of Vertically Aligned Carbon Nanotubes in the Infrared Region, J. Heat Transf. 137 (9) (2015) 091009.
[14] S. Berber, Y.-K. Kwon, D. Tomanek, Unusually high thermal conductivity of carbon nanotubes, Phys. Rev. Lett. 84 (20) (2000) 4613.
[15] T. Ebbesen, H. Lezec, H. Hiura, J. Bennett, H. Ghaemi, T. Thio, Electrical Conductivity of Individual Carbon Nanotubes, 1996.
[16] L. Liu, W. Ma, Z. Zhang, Macroscopic carbon nanotube assemblies: preparation, properties, and potential applications, Small 7 (11) (2011) 1504–1520.
[17] R. Bacon, Growth, structure, and properties of graphite whiskers, J. Appl. Phys. 31 (2) (1960) 283–290.
[18] Y. Yan, M.B. Chan-Park, Q. Zhang, Advances in Carbon-Nanotube Assembly, Small 3 (1) (2007) 24–42.
[19] L. Zhang, X. Wang, W. Xu, Y. Zhang, Q. Li, P.D. Bradford, et al., Strong and Conductive Dry Carbon Nanotube Films by Microcombing, Small 11 (31) (2015) 3830–3836.
[20] W. Bacsa, A. Chatelain, T. Gerfin, R. Humphrey-Baker, L. Forro, D. Ugarte, Aligned carbon nanotube films: production and optical and electronic properties, Science 268 (5212) (1995) 845–847.
[21] Z. Wu, Z. Chen, X. Du, J.M. Logan, J. Sippel, M. Nikolou, et al., Transparent, conductive carbon nanotube films, Science 305 (5688) (2004) 1273–1276.
[22] M. Zhang, S. Fang, A.A. Zakhidov, S.B. Lee, A.E. Aliev, C.D. Williams, et al., Strong, transparent, multifunctional, carbon nanotube sheets, Science 309 (5738) (2005) 1215–1219.
[23] T.T. Tung, C. Pham-Huu, I. Janowska, T. Kim, M. Castro, J.F. Feller, Hybrid Films of Graphene and Carbon Nanotubes for High Performance Chemical and Temperature Sensing Applications, Small 11 (28) (2015) 3485–3493.
[24] D. Zhang, K. Ryu, X. Liu, E. Polikarpov, J. Ly, M.E. Tompson, et al., Transparent, conductive, and flexible carbon nanotube films and their application in organic light-emitting diodes, Nano Lett. 6 (9) (2006) 1880–1886.
[25] S. Huang, Z. Yang, L. Zhang, R. He, T. Chen, Z. Cai, et al., A novel fabrication of a well distributed and aligned carbon nanotube film electrode for dye-sensitized solar cells, J. Mater Chem. 22 (33) (2012) 16833–16838.
[26] Zhao Ce, J. Wu, S. Kjelleberg, J.S.C. Loo, Q. Zhang, Employing a Flexible and Low-Cost Polypyrrole Nanotube Membrane as an Anode to Enhance Current Generation in Microbial Fuel Cells, Small 11 (28) (2015) 3440–3443.
[27] P.-C. Chen, G. Shen, Y. Shi, H. Chen, C. Zhou, Preparation and characterization of flexible asymmetric supercapacitors based on transition-metal-oxide nanowire/single-walled carbon nanotube hybrid thin-film electrodes, ACS nano 4 (8) (2010) 4403–4411.
[28] T. Yamada, Y. Hayamizu, Y. Yamamoto, Y. Yomogida, A. Izadi-Najafabadi, D.N. Futaba, et al., A stretchable carbon nanotube strain sensor for human-motion detection, Nat. Nanotechnol. 6 (5) (2011) 296–301.
[29] H. Chu, Z. Zhang, Y. Liu, J. Leng, Self-heating fiber reinforced polymer composite using meso/macropore carbon nanotube paper and its application in deicing, Carbon 66 (2014) 154–163.
[30] S. Zhang, C. Ji, Z. Bian, R. Liu, X. Xia, D. Yun, et al., Single-wire dye-sensitized solar cells wrapped by carbon nanotube film electrodes, Nano Lett. 11 (8) (2011) 3383–3387.
[31] J. Olivares, T. Mirea, B. Díaz-Durán, M. Clement, M. DeMiguel-Ramos, J. Sangrador, et al., Growth of carbon nanotube forests on metallic thin films, Carbon 90 (2015) 9–15.
[32] Y. Gao, Q. Zhai, R. Barrett, N.S. Dalal, H.W. Kroto, S.F. Acquah, Piezoelectric enhanced cross-linked multi-walled carbon nanotube paper, Carbon 64 (2013) 544–547.
[33] M.N. Uddin, Z.-D. Huang, Y.-W. Mai, J.-K. Kim, Tensile and tearing fracture properties of graphene oxide papers intercalated with carbon nanotubes, Carbon 77 (2014) 481–491.
[34] J. Di, X. Wang, Y. Xing, Y. Zhang, X. Zhang, W. Lu, et al., Dry-Processable Carbon Nanotubes for Functional Devices and Composites, Small 10 (22) (2014) 4606–4625.
[35] E. Snow, P. Campbell, M. Ancona, J. Novak, High-mobility carbon-nanotube thin-film transistors on a polymeric substrate, Appl. Phys. Lett. 86 (3) (2005) 033105.
[36] S. Xiao-gang, Investigation on Radar Absorbing Properties of Carbon Nanotube [J], J. synthetic Cryst. 1 (2005) 010.
[37] Z. Wand, X. Shi, Z. Yu, G. Li, Study on infrared emittance of carbon nanotube coating [J], Ordnance Material Sci. Eng. 1 (2009) 011.
[38] L. Chen, C. Lu, Z. Fang, Y. Lu, Y. Ni, Z. Xu, Infrared emissivity and microwave absorption property of $Sm_{0.5}Sr_{0.5}CoO_3$ perovskites decorated with carbon nanotubes, Mater. Lett. 93 (2013) 308–311.
[39] Q.H.X. Weihao, Research on nanocomposite stealthy materials [J], Aerosp. Mater. Technol. 2 (2002) 002.
[40] P.C.Z.Z.H. Huahui, Study of the materials with low infrared emissivity [J], J. Huazhong Univ. Sci. Technol. 7 (2003) 009.
[41] J. Isenberg, D. Biro, W. Warta, Fast, contactless and spatially resolved measurement of sheet resistance by an infrared method, Prog. Photovoltaics Res. Appl. 12 (7) (2004) 539–552.
[42] D.K. Schroder, Semiconductor Material and Device Characterization, John Wiley & Sons, 2006.
[43] P. Hanselaer, S. Forment, L. Frisson, J. Poortmans, Near IR absorption in diffused layers of Si pn junction solar cells, in: Proc 16th EC-PVSEC, Glasgow, 2000, p. 1348.
[44] D. Schroder, R.N. Thomas, J.C. Swartz, Free carrier absorption in silicon, Solid-State Circuits, IEEE J. 13 (1) (1978) 180–187.
[45] J. Zhang, D. Jiang, H.-X. Peng, A pressurized filtration technique for fabricating carbon nanotube buckypaper: Structure, mechanical and conductive properties, Microporous Mesoporous Mater. 184 (2014) 127–133.
[46] R.L. Whitby, T. Fukuda, T. Maekawa, S.L. James, S.V. Mikhalovsky, Geometric control and tuneable pore size distribution of buckypaper and buckydiscs, Carbon 46 (6) (2008) 949–956.
[47] D.-W. Wang, F. Li, J. Zhao, W. Ren, Z.-G. Chen, J. Tan, et al., Fabrication of graphene/polyaniline composite paper via in situ anodic electropolymerization for high-performance flexible electrode, ACS Nano 3 (7) (2009) 1745–1752.
[48] X. Zhang, F. Shi, X. Yu, H. Liu, Y. Fu, Z. Wang, et al., Polyelectrolyte multilayer as matrix for electrochemical deposition of gold clusters: toward superhydrophobic surface, J. Am. Chem. Soc. 126 (10) (2004) 3064–3065.
[49] M. Zheng, L. Zhang, G. Li, W. Shen, Fabrication and optical properties of large-scale uniform zinc oxide nanowire arrays by one-step electrochemical deposition technique, Chem. Phys. Lett. 363 (1) (2002) 123–128.
[50] Z. Yin, S. Wu, X. Zhou, X. Huang, Q. Zhang, F. Boey, et al., Electrochemical deposition of ZnO nanorods on transparent reduced graphene oxide electrodes for hybrid solar cells, Small 6 (2) (2010) 307–312.
[51] J. Elias, C. Lévy-Clément, M. Bechelany, J. Michler, G.Y. Wang, Z. Wang, et al., Hollow Urchin-like ZnO thin Films by Electrochemical Deposition, Adv. Mater. 22 (14) (2010) 1607–1612.
[52] D.A. Dikin, S. Stankovich, E.J. Zimney, R.D. Piner, G.H. Dommett, G. Evmenenko, et al., Preparation and characterization of graphene oxide paper, Nature 448 (7152) (2007) 457–460.
[53] S. Park, K.-S. Lee, G. Bozoklu, W. Cai, S.T. Nguyen, R.S. Ruoff, Graphene oxide papers modified by divalent ions—enhancing mechanical properties via chemical cross-linking, ACS nano 2 (3) (2008) 572–578.
[54] H. Stahl, J. Appenzeller, R. Martel, P. Avouris, B. Lengeler, Intertube coupling in ropes of single-wall carbon nanotubes, Phys. Rev. Lett. 85 (24) (2000) 5186.
[55] X.-F. Liu, Y.-K. Lai, J.-Y. Huang, S.S. Al-Deyab, K.-Q. Zhang, Hierarchical SiO_2@Bi_2O_3 core/shell electrospun fibers for infrared stealth camouflage, J. Mater. Chem. C 3 (2) (2015) 345–351.
[56] Z. Mao, W. Wang, Y. Liu, L. Zhang, H. Xu, Y. Zhong, Infrared stealth property based on semiconductor (M)-to-metallic (R) phase transition characteristics of W-doped VO_2 thin films coated on cotton fabrics, Thin solid films 558 (2014) 208–214.
[57] Z. Mao, X. Yu, L. Zhang, Y. Zhong, H. Xu, Novel infrared stealth property of cotton fabrics coated with nano ZnO:(Al, La) particles, Vacuum 104 (2014) 111–115.
[58] X.M. Lv, X.L. Gou, H.C. Wang, X.X. Liu, Preparation, Characterization of Low Infrared Emissivity Stealth Coating, in: Advanced Materials Research; 2013, Trans Tech Publ, 2013, pp. 2502–2505.